

PAPER • OPEN ACCESS

Interpretive modelling of boron transport in the boundary plasma of WEST experiments with the impurity powder dropper












To cite this article: K. Afonin *et al* 2023 *Nucl. Fusion* **63** 126057

View the [article online](#) for updates and enhancements.

You may also like

- [Convective end effects in annular linear induction pumps](#)
Yves Delannoy, Elena Martin-Lopez and Fabrice Benoit
- [Edge turbulence in ISTTOK: a multi-code fluid validation](#)
B D Dudson, W A Gracias, R Jorge et al.
- [Long plasma duration operation analyses with an international multi-machine \(tokamaks and stellarators\) database](#)
Xavier L Litaudon, Hans-Stephan Bosch, Tomohiro Morisaki et al.

Interpretive modelling of boron transport in the boundary plasma of WEST experiments with the impurity powder dropper

K. Afonin^{1,*} , A. Gallo¹ , Y. Marandet² , Ph. Moreau¹, G. Bodner³ , H. Bufferand¹, G. Ciraolo¹, C. Desgranges¹, P. Devynck¹ , A. Diallo² , J. Gaspar⁴ , C. Guillemaut¹, R. Guirlet¹ , J.-P. Gunn¹, N. Fedorczak¹, T. Loarer¹, R. Lunsford³ , P. Manas¹, F. Nespoli³ , N. Rivals², P. Tamain¹, E.A. Unterberg⁵  and the WEST Team^a

¹ CEA, IRFM, F-13108 Saint-Paul-Lez-Durance, France

² Aix-Marseille Univ, CNRS, PIIM, Marseille, France

³ Princeton Plasma Physics Laboratory, Princeton, NJ, United States of America

⁴ Aix Marseille Univ, CNRS, IUSTI, Marseille, France

⁵ Oak Ridge National Laboratory, Oak Ridge, TN 37830, United States of America

E-mail: Kirill.AFONIN@cea.fr

Received 14 June 2023, revised 2 October 2023

Accepted for publication 20 October 2023

Published 6 November 2023



Abstract

Boron (B) powder injection is a potential alternative to glow discharge boronization as a wall conditioning method for tokamaks. This technique is currently being studied in WEST experiments, during which B powder is injected by an Impurity Powder Dropper developed by PPPL. In order to interpret and analyse experimental trends, and to help develop future experiments, a modelling workflow using a boundary plasma simulation (SOLEGE-EIRENE) and powder ablation simulation (Dust Injection Simulator) was developed and tested. The effect of adding a B neutral source to simulated deuterium + oxygen (D + O) plasmas was compared to experimental data from the WEST C5 campaign, where B powder was injected in a dedicated experiment. While the impact of B injection on radiated power P_{rad} measurements at the upper divertor was similar, there were significant differences in measurements of P_{rad} , outer strike point electron temperature T_e^{OSP} and O-II line intensity at the lower divertor between experiment and simulation. This discrepancy suggests that those parameters were affected by phenomena not present in the simulations, with the most likely candidates being reduced D recycling and a reduced O sourcing from the divertor.

Keywords: magnetic fusion, plasma-wall interaction, wall conditioning, boundary plasma modelling, impurity powder dropper, WEST

(Some figures may appear in colour only in the online journal)

^a <http://west.cea.fr/WESTteam>.

* Author to whom any correspondence should be addressed.



Original content from this work may be used under the terms of the [Creative Commons Attribution 4.0 licence](https://creativecommons.org/licenses/by/4.0/). Any further distribution of this work must maintain attribution to the author(s) and the title of the work, journal citation and DOI.

1. Introduction: preliminary Impurity Powder Dropper (IPD) experiments in WEST

The tungsten (W) Environment in Steady-state tokamak (WEST) [1, 2] utilizes almost exclusively W plasma-facing components (PFCs) to validate their use in ITER and future pilot plants. While W PFCs have a higher melting point, heat conductivity, and lower retention of the hydrogenic species than carbon PFCs, they can contaminate the plasma with high Z impurities. This leads to large radiative losses in the confined plasma, which degrades tokamak performance by lowering the central electron temperature. In a pilot plant, this loss of performance can lead to a lowered fusion reaction rate and possibly a disruption. One of the methods to mitigate W contamination is to condition the PFCs with low-Z coatings as is done in glow discharge boronization (GDB) [3, 4], which deposits layers of boron (B) onto the PFCs with a glow discharge seeded with a B-enriched gas such as B_2D_6 or B_2H_6 . To ensure uniform distribution, the magnetic field coils have to be shut down during GDB, which presents a conflict for superconducting devices (such as ITER) that have constraints on their toroidal field duty cycle. Lastly, B_2D_6 gas is toxic which adds additional safety concerns and costs. For these reasons, future reactors will need other methods of wall conditioning.

An alternative method of wall conditioning is currently being studied on a number of different tokamaks and stellarators: injection of low-Z powder during the plasma discharge. A device named the IPD was developed by the Princeton Plasma Physics Laboratory [5] to test this real-time wall conditioning technique. Results of the first deployment of the IPD on WEST are detailed in [6]. Time traces of line-averaged n_e , input LH heating power P_{LH}^{total} , total radiated power P_{rad}^{total} and O-II visible line spectroscopy measurements are given in figure 1.

In those experiments B powder was injected into ten lower single-null (LSN) L-mode discharges with the following characteristics: toroidal field $B_T = 3.7$ T, lower hybrid current drive power $P_{LHCD} \sim 4.5$ MW, and volume-averaged electron density $n_e \sim 3.5 \times 10^{19} \text{ m}^{-3}$. For each discharge, the B drop rate was varied to determine the largest amount of B that could be dropped without triggering a disruption. The maximum tolerated drop rate was found to be $9 - 17 \text{ mg s}^{-1}$ for that series of discharges, with 310 mg of B injected over the whole commissioning experiment.

Measurements obtained in those experiments are used here for modelling analysis of B transport, both as a source of the input parameters to setup the simulated experimental conditions (e.g. outer midplane electron density n_e^{outer} , n_e and T_e profiles at the divertor) as well as a reference for the simulated impact of B injection (e.g. bolometry and spectroscopy measurements). Measurements from the following diagnostics were employed: embedded Langmuir probes mounted at the lower divertor for the measurements of electron density (n_e) and temperature (T_e) [7], midplane fast-sweep reflectometry for the boundary n_e radial profile [8], visible spectroscopy for impurity line emission at the lower outer divertor and at the midplane antenna limiter [9], and bolometry for radiated

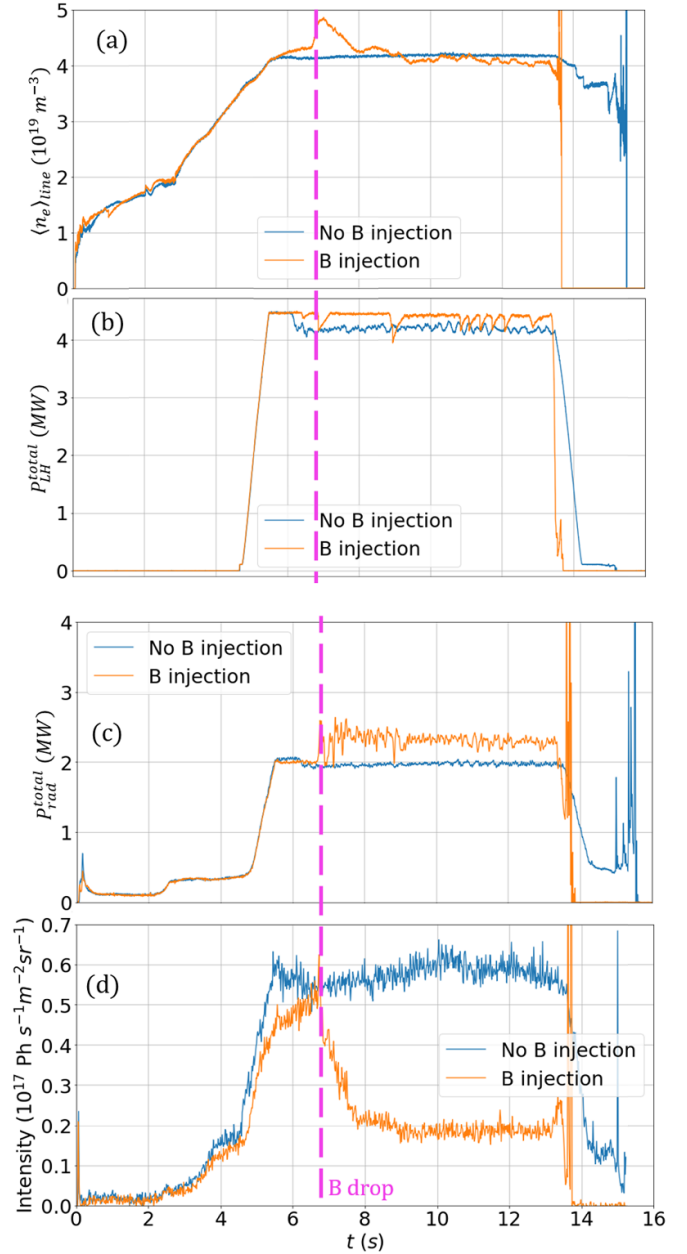


Figure 1. Time traces from two shots (control and with B powder injection) of IPD experiment on WEST: (a) line-average n_e along equatorial line of sight; (b) total LH input power; (c) total radiated power; (d) O-II ($\lambda = 441.5 \text{ nm}$) visible line intensity at the outer strike point, lower divertor.

power (P_{rad}) [10, 11]. Notably, visible spectroscopy data for the upper divertor was not available for this experiment, so the ratio of B line emission from the upper divertor to the emission from the lower divertor, as well as any such ratio for any other element could not be measured.

In order to better interpret the experimental data and to help design future experiments it is necessary to model the transport of injected B in the WEST boundary plasma. The main goal of modelling is to study the distribution of B incident flux on the PFCs. For this reason, a novel modelling workflow was developed and tested, and the results are

described in this paper. Section 2 outlines the architecture of the modelling workflow. Section 3 describes the modelling results for a series of simulations. Section 4 compares the impact of B injection in experiment to the simulated impact of the added B neutral source. Section 5 concludes and provides a plan for future work with the developed workflow.

2. Modelling workflow for IPD experiments

Previous attempts have been made to simulate the transport of impurities introduced through powder injection [12–16]. In [12], a pure deuterium (D) boundary plasma was modelled with the EMC3-EIRENE [13] code suite, and then used as an input for the DUST Transport (DUSTT) code [14]. DUSTT in turn provided trajectories and evaporation rates for the B spherical particles. B transport and plasma-surface interactions were then modelled using ERO2.0 [15]. Another approach is described in [16], where EMC3-EIRENE was used exclusively, with a point source of atomic B placed in the upper part of the boundary plasma. In both cases, the plasma was considered to have no impurities other than B, and EMC3 treated impurities under the trace approximation, i.e. while impurity radiative losses were taken into account when calculating plasma temperature, they did not contribute to charge balance. The effect of impurities on the main plasma was therefore not completely self-consistent.

In our study, we approached the problem in a similar way to [12], with SOLEDGE-EIRENE [17] calculating the boundary plasma and modelling B transport, and Dust Injection Simulator (DIS) code [18] modelling powder dynamics and ablation. SOLEDGE-EIRENE allows us to model plasma up to the first wall everywhere in the poloidal cross-section, which enables us to calculate B incident flux on the entirety of the wall contour. DIS was recently used to model powder injection experiments on LHD using EMC3-EIRENE plasma backgrounds in [19]. For the plasma before B injection (pre-drop phase), two elements were modelled: D as the main ion species, and oxygen (O) as a proxy for all light impurities present before B injection, which are usually O, carbon and nitrogen. Using an additional light impurity, like O, allows for a better match of the electron temperature and radiated power measurements from experiment. Eight species of O were modelled, one for each ionization state. The modelling workflow was separated into three steps: (i) modelling of the pre-drop phase of the discharge, (ii) modelling of B particle ablation and evaporation with plasma parameters from the pre-drop phase and (iii) modelling of the drop phase of the discharge with the neutral B volumetric source provided by the B particle simulation from step (ii). pre-drop and drop phases of a simulation refer to steady-state SOLEDGE-EIRENE solutions, which corresponded to the experimental plasma conditions in the middle of the flat-top phase before and during B powder injection. The effects of B injection on the modelled plasma were then compared to the effects of B injection observed in experiment. While the most recent version of

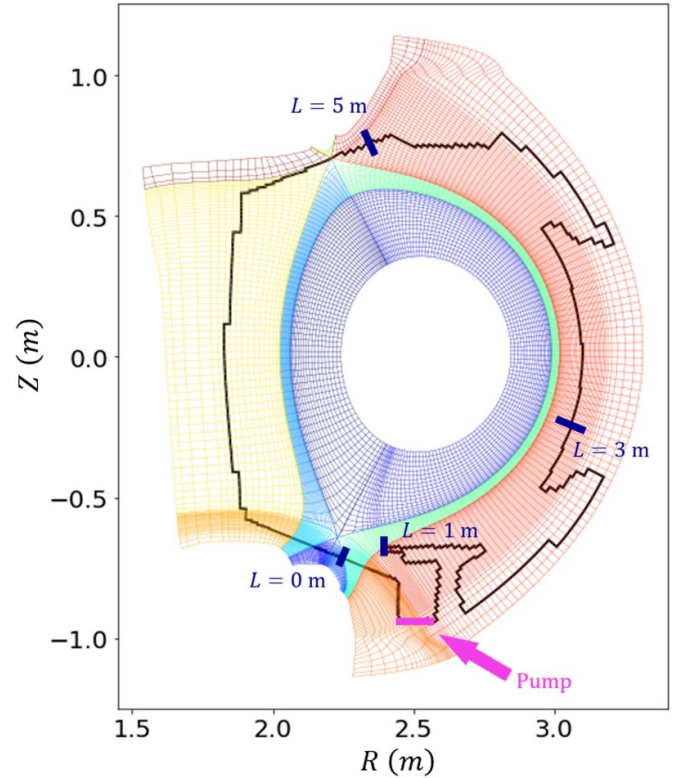


Figure 2. Quadrangular simulation mesh for SOLEDGE-EIRENE with the pump location shown in magenta and wall coordinate ticks shown in dark blue.

SOLEDGE-EIRENE code suite supports 3D modelling [20], only 2D simulations were carried out and analysed in this preliminary study. Moreover, dynamics of plasma-wall interactions were not modelled, thus the reduction of D recycling due to B deposition on the PFCs and the erosion of W PFCs was not taken into account. Additionally, the B recycling coefficient was assumed to be zero (i.e. B was assumed to ‘stick’ to the PFCs on which it was deposited). For D and O, the recycling coefficients were set to 0.95 for the pump under the baffle and 1.0 for the rest of the wall. No cross-field drifts were assumed in this analysis.

Figure 2 depicts the simulation domain for SOLEDGE-EIRENE. The simulation grid was built based on the magnetic equilibrium reconstruction of WEST discharge 56 919 from the NICE reconstruction code [21]. The walls were considered to be made of pure W with the pump located under the baffle. Since the plasma in this study was modelled in 2D, the geometry of the wall contour was assumed to be axisymmetric. In reality, WEST has toroidally localized antennae that act as poloidal limiters, which cannot be accurately described by a 2D model. The antennae have a toroidal length of approximately 30° , so in order to have a compromise in terms of the recycling flux and cooling effect on the plasma, the portion of the wall contour that represents the antennae is placed at major radius $R^{\text{LHCD}} = 3.1$ m, further away from the separatrix with respect to its actual radial position in the modelled experiment. This working assumption is consistent with previous

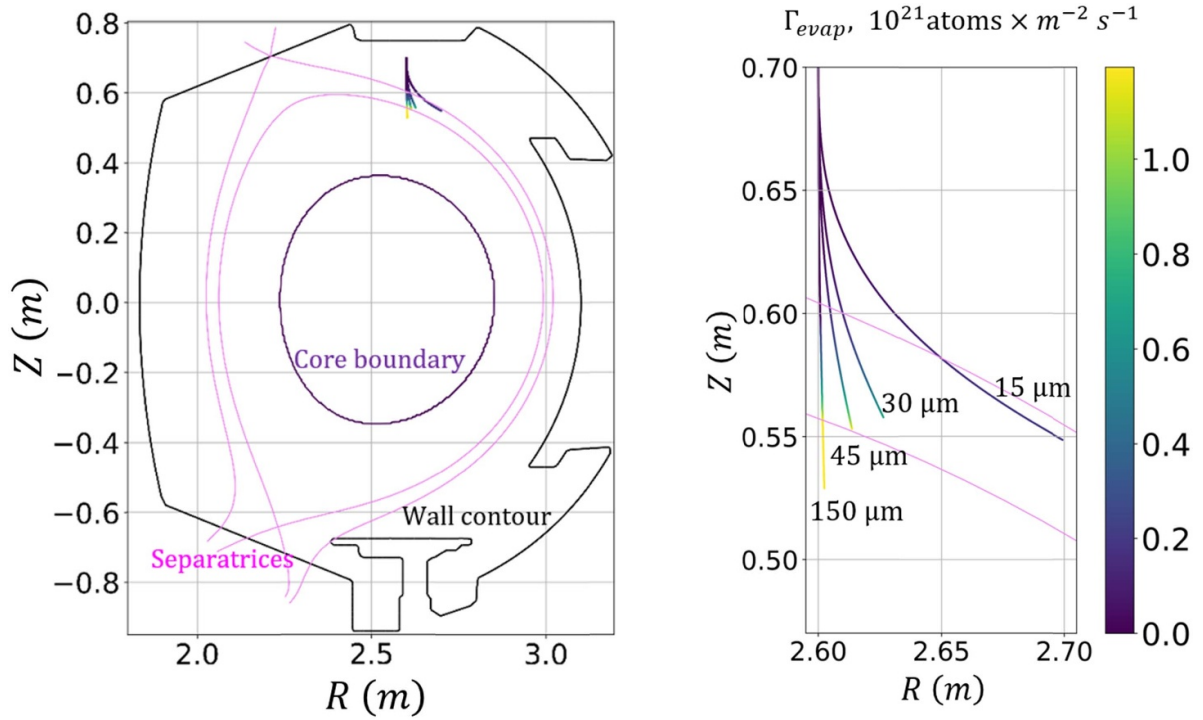


Figure 3. Particle trajectories from DIS for B particles of varying diameters (15–150 μm) with the evaporation flux Γ_{evap} shown in colour (a.u.).

WEST modelling efforts [22–24]. The inner boundary of the simulation domain was placed far from the separatrix in the confined plasma to model B transport in edge plasma, since there was evidence from the VUV spectroscopy (increase of 24.3 nm B-V line intensity) that B may be transported into the confined plasma [6].

To match pre-drop phase simulation results with experimental data, as well as to analyse the effect of plasma conditions on the B distribution, two techniques were used. First, the D particle diffusion coefficient D_n^D was modified during the simulation with a feedback scheme on the outer midplane density profile n_e^{omp} , allowing it to be fit with pre-drop phase experimental measurements. The O diffusion coefficient D_n^O was set to $0.5 \text{ m}^2 \text{ s}^{-1}$ across the whole simulation domain. Second, the input power P_{in} and O source (in the form of a core boundary condition on the total O density $n_{\text{O}}^{\text{core}}$) were varied over a range of values to scan the parameter space for further analysis. The perpendicular heat diffusivity coefficient $\chi_{i,e}$ was assumed to be constant and equal to $4.0 \text{ m}^2 \text{ s}^{-1}$.

After calculating a set of D + O boundary plasma simulations for the pre-drop phase, we used DIS to calculate the spatial distribution of the B source for each simulation. Plasma parameters from a given D + O simulation (densities and temperatures of electrons, ions and neutrals $(n, T)_{e,i,n}$, Mach number \bar{M}) were axisymmetrically extrapolated in 3D, and a spherical particle was launched vertically downward from the top of the machine, as shown in figure 3. The injection point was at $R_{\text{inj}} = 2.6 \text{ m}$ and $Z_{\text{inj}} = 0.7 \text{ m}$. Here, a single B

sphere represented a multitude of B grains dropped in the experiment. The injection point had approximately the same coordinate as the end of the IPD tube. The diameter of the particle was $d_{\text{part}} = 150 \mu\text{m}$ which matched the size of the powder utilized in the experiment. Figure 3 also shows the impact of particle size (15–150 μm) on the trajectory of B test particles for a simulation with $P_{\text{in}} = 3 \text{ MW}$ and O relative concentration $C_{\text{O}}^{\text{core}} = 2.83\%$ (described in section 3). Larger particles tended to penetrate the boundary plasma further and reach closer to the core as they were dragged outwards less by the centrifugal forces. Similar results were observed in [12].

To model the drop phase of the plasma discharge, a source of neutral B atoms was added to the SOLEDGE-EIRENE simulation based on the evaporation rate calculated by DIS and scaled according to the desired powder injection rate. Total evaporation of the injected powder was assumed at this step. The B neutral source was assumed to be distributed axisymmetrically. The injected mass rate was varied from 2.5 to 9.2 mg s^{-1} and the particle diffusion coefficient D_n^B was set to $0.5 \text{ m}^2 \text{ s}^{-1}$ (same as D_n^O).

Input parameters described above were chosen to try to qualitatively match the simulated plasma with the measurements from the IPD experiment, for example plasma discharge #56 919. At the same time, the goal of the modelling analysis described in this paper is to perform scans of various input parameters to extract general trends that could inform future WEST experiments. Therefore, rather than trying to precisely

Table 1. Parameters for pre-drop simulations in SOLEDGE-EIRENE.

Input power P_{in} , MW	2.75	2.875	3.0
O core boundary concentration n_O^{core} , $10^{17}m^{-3}$	7.582	8.3402	9.0984
O core relative concentration $C_O^{core} = n_O^{core}/n_D^{core}$, %	2.36%	2.59%	2.83%

reproduce a given WEST discharge, we aim to estimate the impact of various plasma parameters on B distribution.

3. Modelling results

A set of nine pre-drop simulations were run with varying P_{in} and n_O^{core} values, given in table 1. To match simulations with experimental data, P_{in} in the simulation should equal $P_{heating} - P_{rad}^{core}$ from the experiment. Here, $P_{heating}$ is the total heating power in the experiment and P_{rad}^{core} is the radiated power emitted by a portion of the plasma in the core region with the same boundary as the core boundary in the simulation. P_{rad}^{core} was approximated with $P_{rad}^{bulk} = P_{rad}^{total} - P_{rad}^{div}$, where P_{rad}^{div} is the radiated power measured by bolometers targeting both divertors (chords 1–3, 14, 15 in figure 5 in [10]). In the case of the pre-drop phase in shot 56 919 $P_{rad}^{bulk} \approx 1.9$ MW, therefore $P_{in} \approx P_{heating} - P_{rad}^{bulk} = 2.6$ MW. For the simulations, we chose three values of P_{in} above this estimation, since P_{rad}^{bulk} is an overestimation of P_{rad}^{core} due to midplane bolometry lines of sight (LOS) passing through midplane section of the scrape-off layer (SOL). The effect of the input parameter C_O^{core} on the overall C_O spatial distribution is shown in figure 4: here C_O is normalized by the ratio between C_O^{core} for a given run and the lowest C_O^{core} used in the scan (2.36%), for improved comparability. If in the rest of the simulation domain (not shown) the normalized C_O is almost identical for the three runs, the only region showing a significant change is the far SOL of the inner divertor plasma, as highlighted by the magenta circle in panels (a)–(c).

One of the goals of the pre-drop phase plasma modelling was to qualitatively match the simulated plasma parameters with those measured in the experiment. Figure 5 shows experimental data for shot 56 919 with the parameters from a selected subset of simulations to show the sensitivity of different plasma parameters due to the variation of input parameters. Figure 5(a) shows n_e^{outer} from the pre-drop phase with the simulated densities. Modelled n_e^{outer} changes minimally with C_O^{core} and P_{in} and generally matches the measurements, especially in the plasma edge region. The discrepancy in the SOL region might be caused by the unitary recycling coefficient for D and O (1.0 in all simulations). The feedback loop on the diffusion coefficient in SOLEDGE attempts to match profiles with a feedback algorithm, providing an approximate diffusion coefficient map, so there is no guarantee from the algorithm to reach the target n_e profile. Methods to improve this feedback mechanism and, therefore, the match between simulated

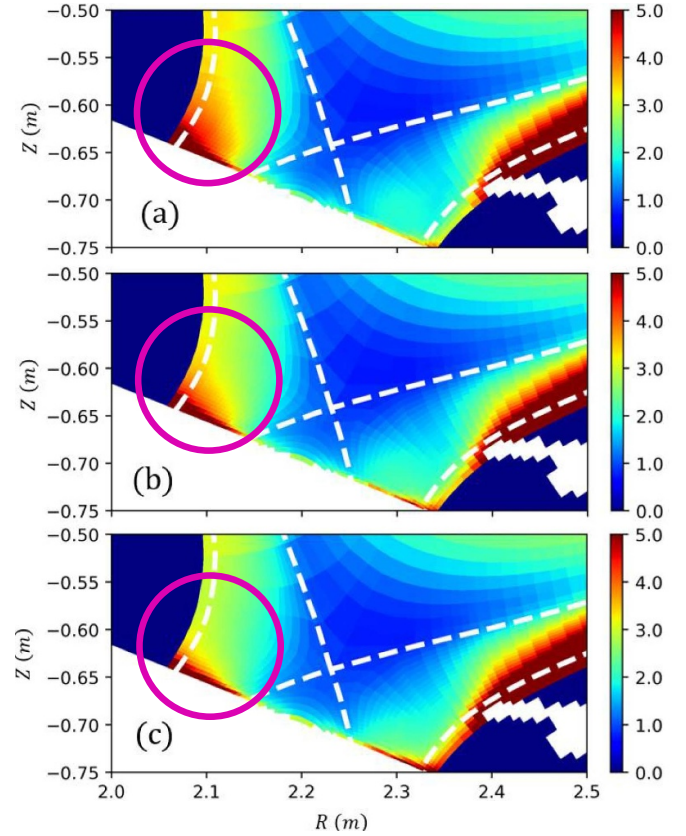


Figure 4. Normalized O concentration $C_O \times \left(\frac{C_O^{core}}{2.36\%}\right)^{-1}$ for simulations with the input power $P_{in} = 2.875$ MW and $C_O^{core} =$ (a) 2.36%, (b) 2.59%, (c) 2.83%. The spatial distribution of C_O remains essentially unchanged with increasing C_O^{core} , with the exception of the far SOL on the HFS (highlighted with a magenta circle).

and measured n_e will be investigated in future efforts. This discrepancy can affect the atomic processes of light impurities, which in turn would affect impurity distribution and synthetic diagnostic data in pre-drop and drop phase simulations. However, the goal of this study is to predict general trends of B distribution in the plasma and B influx distribution on the PFCs rather than trying to reproduce a given WEST discharge. Figures 5(b) and (c) compare experimental and modelled T_e^{OSP} and n_e^{OSP} . Here, the discrepancies are more pronounced. These can be resolved by lowering P_{in} to match the measured T_e^{OSP} , which was done in [25], but that led to additional inconsistencies (e.g. in the outer midplane density). Figures 5(d) and (e) compare averaged bolometry signals S from the pre-drop phase (from $t = 5.6$ s to $t = 6.6$ s) of the experiment with those from simulations calculated with the SYNDI synthetic diagnostic [26] for the same set of SOLEDGE-EIRENE simulations. Lines of sight of the bolometer are shown on the figure 6.

SYNDI calculates synthetic bolometry signals by multiplying 2D maps of emissivity provided by a SOLEDGE-EIRENE mask with weight coefficients for each LOS from a given diagnostic. The resulting matrix is then integrated to obtain

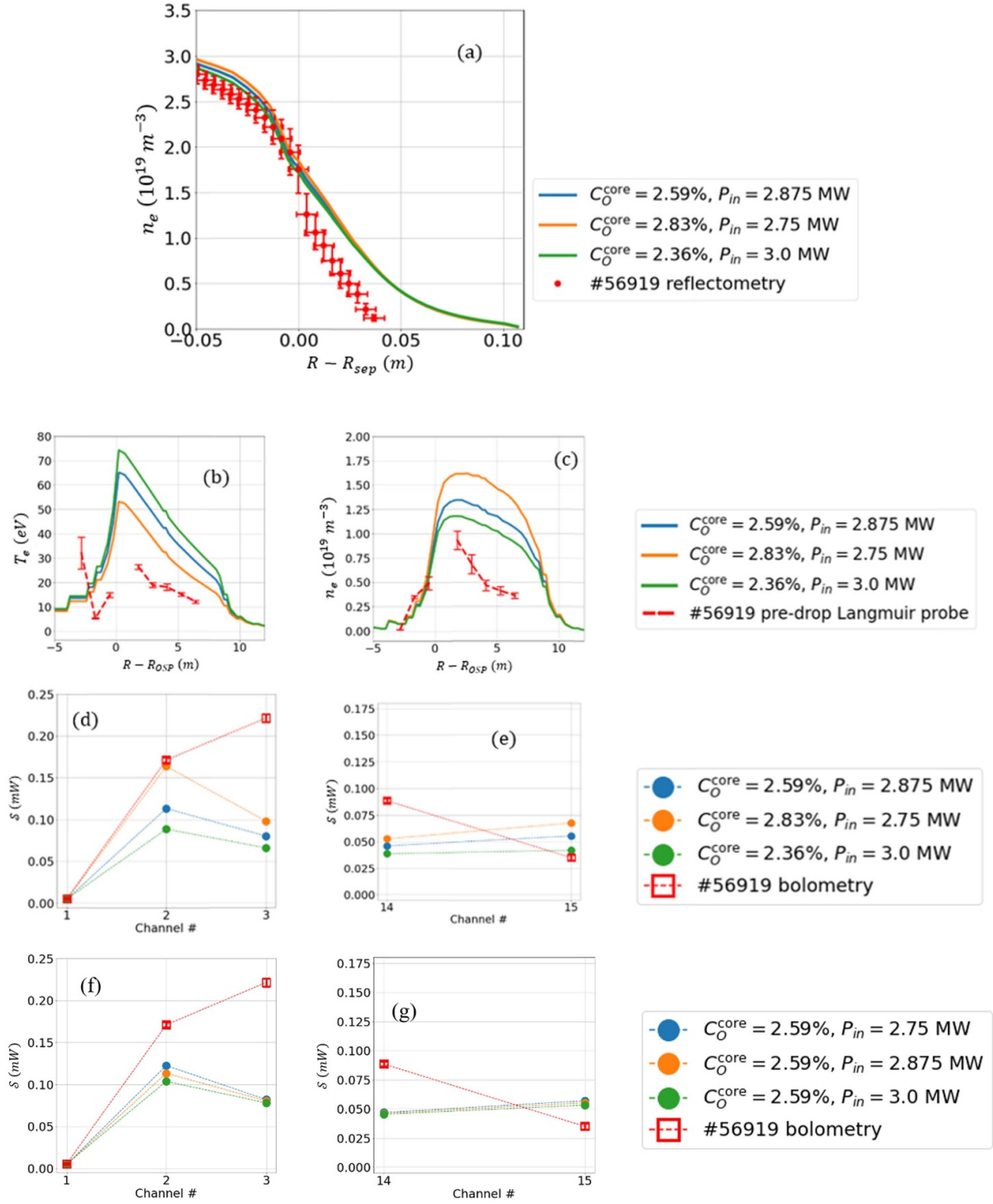


Figure 5. Comparison of simulated (solid lines) and experiment measurements (dots with error bars): (a) outer midplane density n_e^{outer} from three simulations and fast sweep reflectometry data from the experiment; (b) outer strike point temperature T_e^{OSP} wall profiles from a subset of simulations and reciprocating Langmuir probe measurements of T_e^{OSP} in the experiment; (c) same as (b) but for the outer strike point density n_e^{OSP} ; (d), (e) bolometry signals S for boundary channels in pre-drop phase (red boxes with error bars) and SYNDI Measurements in SOLEDGE-EIRENE simulations at the upper and lower divertor; (f), (g) same as (d), (e) but with the variation of P_{in} only.

the synthetic measurement for a given LOS. Figure 6 shows the P_{rad} map for one of the simulations with five lines of sight from bolometry, three for the lower divertor and two for the upper divertor. These lines of sight were chosen because they

only go through the boundary plasma. Since O was the only impurity in the simulation, we chose to compare experimental and synthetic bolometry signals from the boundary plasma in order to match the light impurity content. The experimental

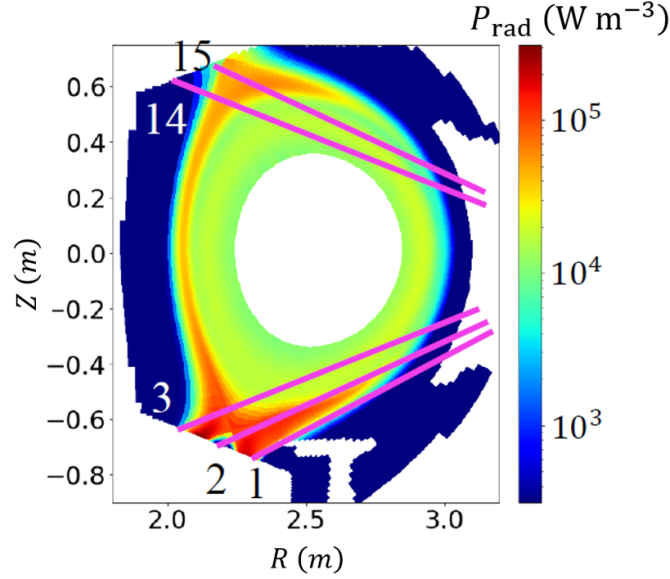


Figure 6. Radiated power map for one of the simulations with five lines of sight of bolometry (input power $P_{in} = 2.875$ MW, core O concentration $C_O^{core} = 2.59\%$) with SYNDI lines of sight in magenta that correspond to the positions of bolometry lines of sight in WEST.

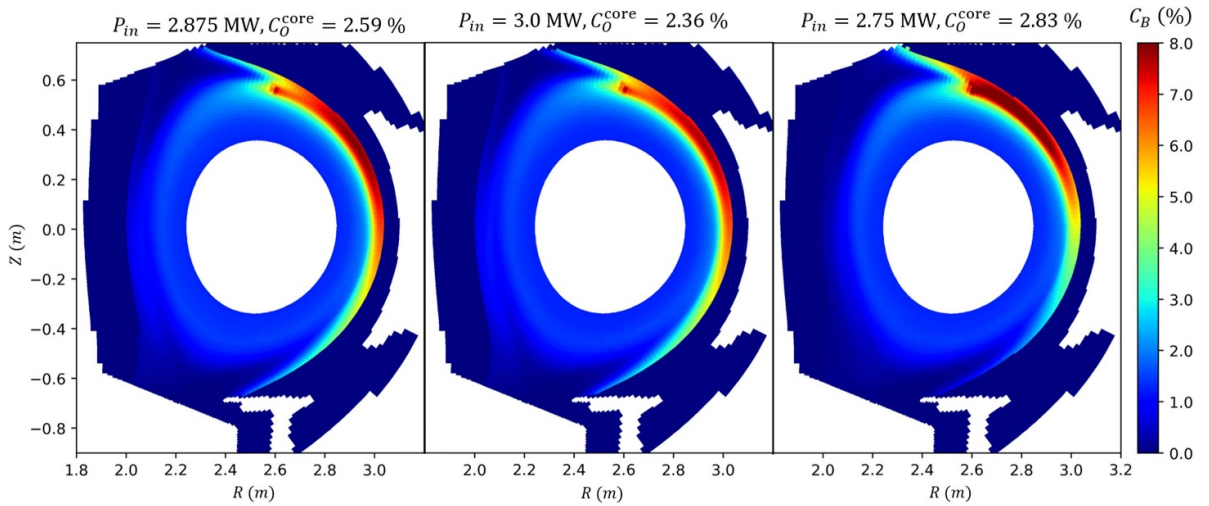


Figure 7. 2D map of relative concentration $n_B^{\Sigma ions}/n_e$ for a set of simulations.

trend in bolometry signals was not qualitatively reproduced by SOLEDGE, which may be due to different impurity profiles in the simulations and the experiment. Increasing P_{in} led to a decrease in SYNDI bolometry signal, all other parameters being equal (figures 5(f) and (g)), which is caused by the decrease of O radiative cooling rate L_Z^O with the increase of T_e : $\frac{d(L_Z^O)}{d(T_e)} < 0$, $T_e \in [20 \text{ eV}, 80 \text{ eV}]$ [27], and T_e in SOL is in this range in the simulations.

To model the boron drop, varying amounts of B powder (mass rate $\mu_B = 2.3, 4.6 \text{ mg s}^{-1}$) were injected into the simulations described above. Figure 7 shows the 2D maps of the relative B concentration $n_B^{\Sigma ions}/n_e$ for three simulations, which remained relatively unchanged despite different levels of C_O^{core} and P_{in} .

The first goal of the modelling analysis was to investigate the effect of modified plasma parameters on B flux distribution

to the PFCs. To achieve this, the normalized total B incident flux was calculated for each drop phase simulation:

$$\Gamma_B^{norm} = \Gamma_B(L) / \int \Gamma_B(L) dL.$$

Where $\Gamma_B = \sum_{i=0}^5 \Gamma_B^i$, L is the wall contour length, Γ_B^i is the wall incident flux of B in the i th ionization state for $i > 0$ and the neutral B wall incident flux for $i = 0$. One-dimensional plots of $\Gamma_B^{norm}(L)$ along the wall are given in figure 8 for different sets of input parameters. In general, the Γ_B^{norm} distribution stayed approximately the same for the variations in P_{in} , μ_B and C_O^{core} , with B being spread more homogeneously at higher P_{in} and lower μ_B , all other parameters being equal. Interestingly, in all of the drop phase simulations, the upper divertor received a substantial amount of B with respect to Γ_B^{norm} on the lower

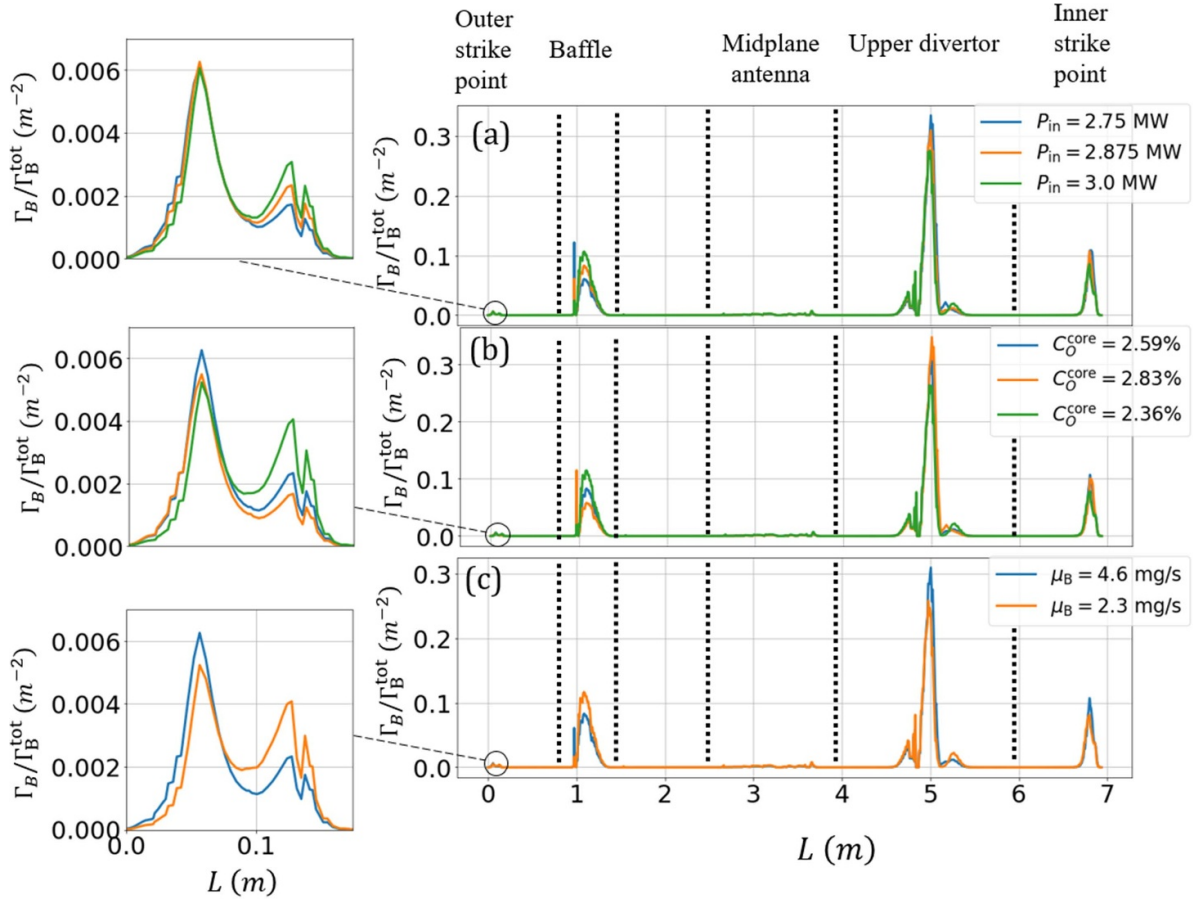


Figure 8. Normalized distribution of B total incident flux summed over all B species Γ_B^{norm} for drop phase simulations with the variations of: (a) input power P_{in} , with O core concentration $C_O^{\text{core}} = 2.59\%$ and B mass rate $\mu_B = 4.6 \text{ mg s}^{-1}$ (b) C_O^{core} , $P_{\text{in}} = 2.875$ and $\mu_B = 4.6 \text{ mg s}^{-1}$ (c) μ_B , $C_O^{\text{core}} = 2.59\%$ and $P_{\text{in}} = 2.875$.

divertor. A difference of 1.5–4 times between the integrated incident fluxes of B ions and neutrals to the upper and lower divertors was estimated despite the LSN configuration. This ratio increased for smaller P_{in} and higher μ_B . Experimental validation of this influx ratio remains unsolved due to the lack of visible spectroscopy data during the C5 campaign. Future experiments on WEST will feature larger visible spectroscopy coverage at the upper divertor to test this hypothesis.

The modelling results also suggested that the OSP received little to no injected B when compared to the other affected PFCs such as the baffle region. In contrast, the experiment observed similar levels of B-II line brightness at the baffle and the OSP, show in figure 9. Spectroscopy measurements from the experiment could not be compared with the synthetic diagnostic data from simulations provided by SYNDI as there was no inclusion of B recycling in the model. Therefore, there were practically no B⁺ ions at the lower divertor, as B⁺ ions were only present in the vicinity of neutral B source. Future modelling should include a non-zero recycling coefficient for B, which might affect Γ_B^{norm} distribution. Lastly, the lack of B at the OSP might be an indication of incomplete transport dynamic of B such as a lack of radial electric field or assumption of axisymmetry of B source, which must be addressed in future modelling.

4. Comparative analysis of B injection in modelling and experiments

Having modelled both pre-drop and drop phases, we compared the impact of B injection in the experiments with the impact of adding a B source in the simulations. For example, we compared the difference between bolometry signals in the pre-drop and drop phases in the experiments to the same difference in the synthetic bolometry signals from the simulations. For bolometry, SYNDI was applied to the P_{rad} 2D maps. Figure 10 shows bolometry signals \mathcal{S} for plasma simulations as well as experimental values for the same signals from shot #56 919 in the drop phase and the ratio between them and the signals from the pre-drop phase, that were shown in figures 4(d) and (e). The rows of the figure 10 show $\mathcal{S}^{\text{low,up}}$ from lines of sight targeting lower and upper divertor respectively. The columns show \mathcal{S} for two drop rates in modelling as well as measured bolometry signals in the experiment, with average value and standard deviation calculated before and after B injection. The figure 11 shows ratios of the signals $(\frac{\mathcal{S}_{\text{drop}}}{\mathcal{S}_{\text{pre-drop}}})^{\text{low,up}}$ described above.

The effect of B injection on bolometry signals were qualitatively reproduced at the upper divertor for both pre-drop and drop phases, especially with higher μ_B . In particular, synthetic

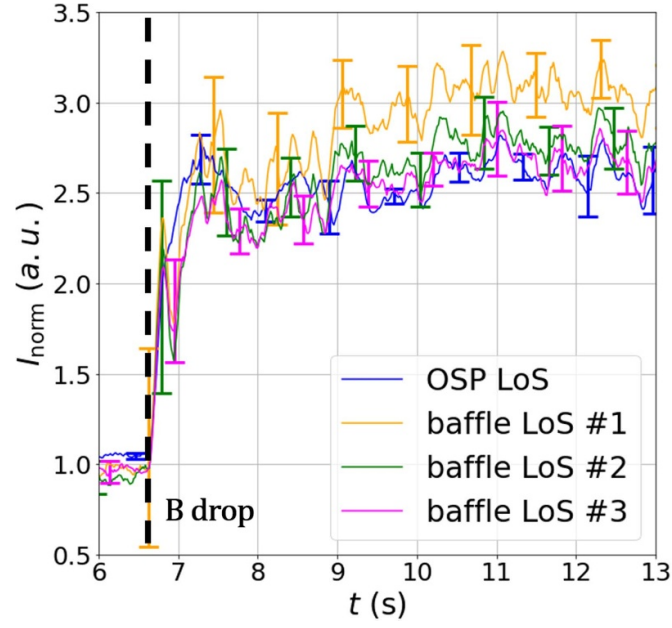


Figure 9. Line intensity of B-II ($\lambda = 419.5$ nm) in the experiment at the baffle and OSP, normalized by pre-drop values.

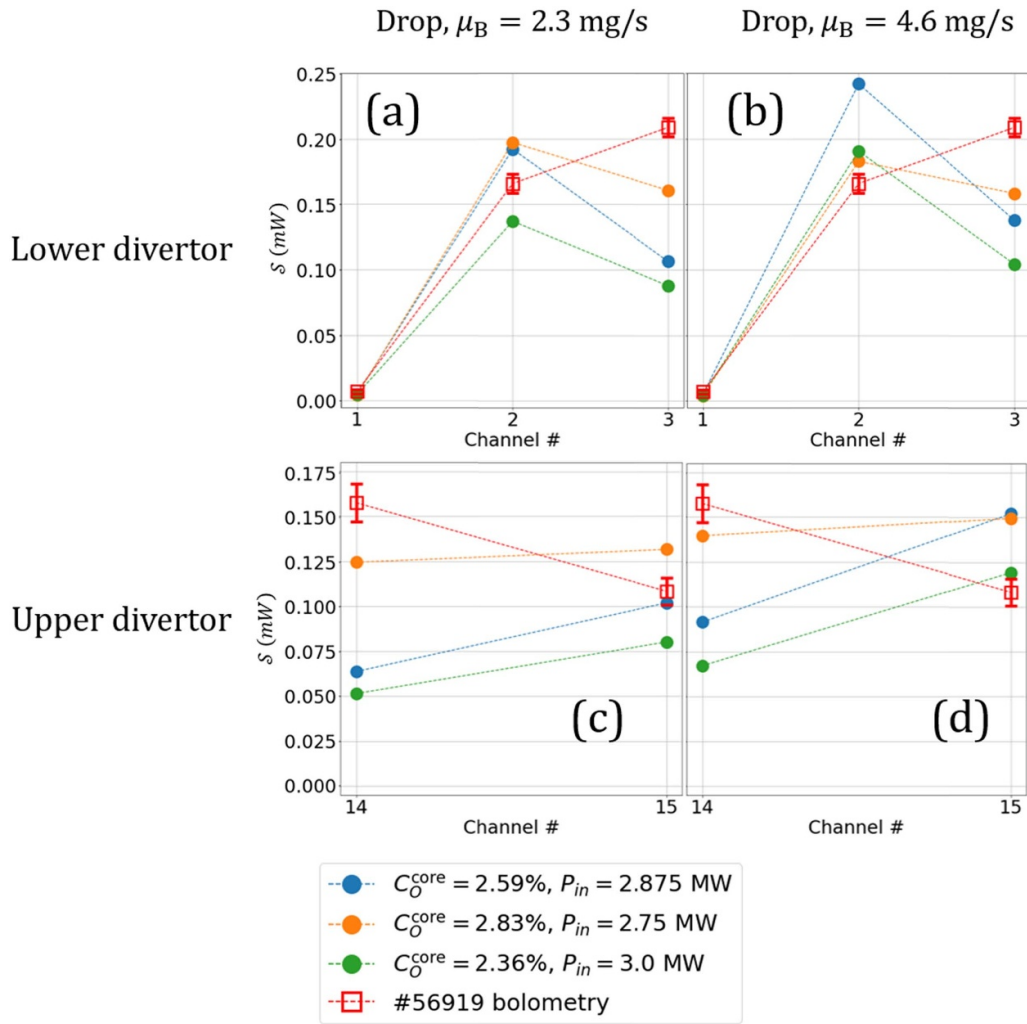


Figure 10. Bolometry channel output signals S from the experiment (red boxes) and calculated with SYNDI for studied simulations (dots): (a), (b) signals at the lower divertor for the drop phase with B mass rate $\mu_B = 2.3, 4.6$ mg s $^{-1}$ respectively; (c), (d) same, for the upper divertor.

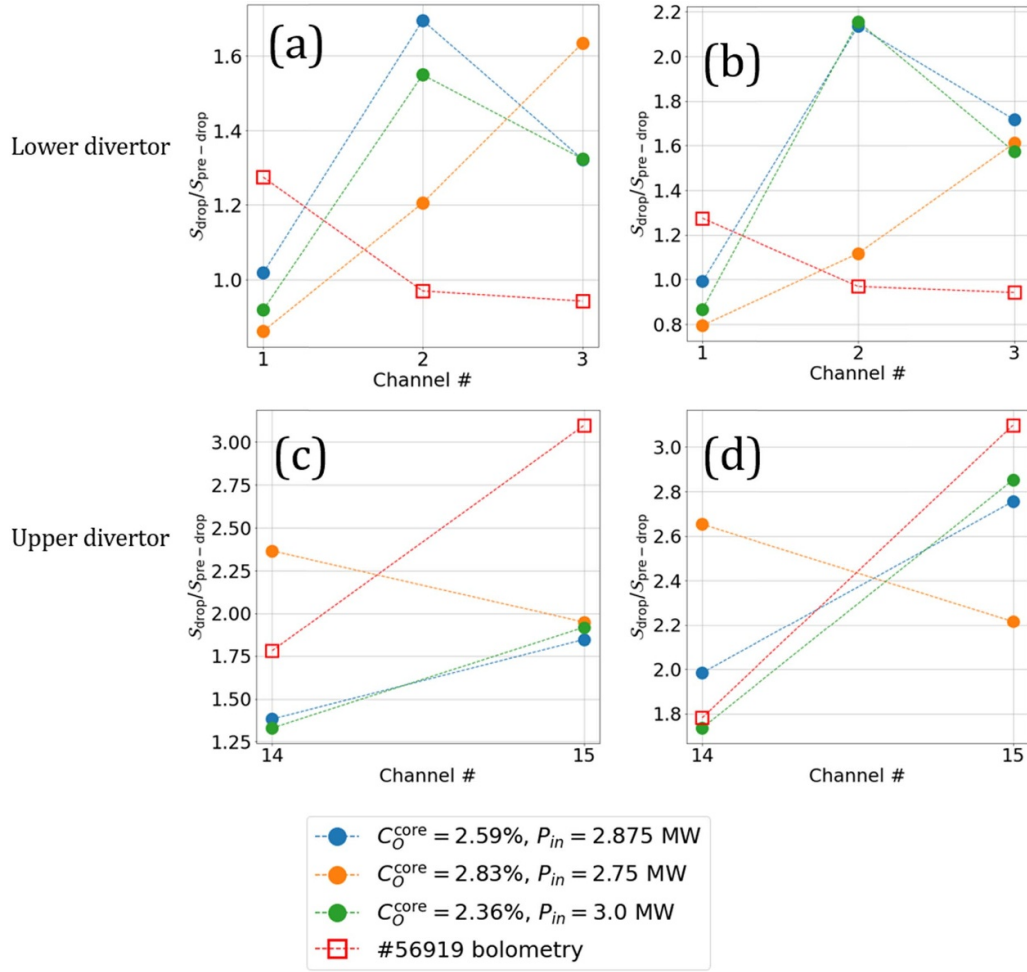


Figure 11. Bolometry signal ratios $\frac{S_{\text{drop}}}{S_{\text{pre}} - \text{drop}}$ from the experiment (red boxes) and calculated with SYNDI for studied simulations: (a), (b) $\frac{S_{\text{drop}}}{S_{\text{pre}} - \text{drop}}$ for B mass rate $\mu_B = 2.3, 4.6 \text{ mg s}^{-1}$ for the lower divertor; (c), (d) same for the upper divertor.

bolometry signals for simulations with higher μ_B at the upper divertor show a 2–3 times increase, similar to bolometry measurements increase in the experiment. Discrepancy between channels 14 and 15 in modelling and experiments could be attributed to an inaccurate representation of magnetic equilibrium in the upper part of the vessel caused by the mapping of reciprocating Langmuir probe (RLP) data along the magnetic flux surfaces, which can result in the uncertainty in the radial direction [22].

At the lower divertor, the impact of B injection on experimental and synthetic bolometry signals greatly differ, shown in figures 11(a) and (b). Synthetic signals increased for channels 2 and 3 and decreased for channel 1; while in experiment, the bolometry signals remained approximately constant. The channel 1 signal behaviour may be explained by the sensitivity of the model to near-target plasma parameters and by lower light impurity concentration near OSP relatively to volume near ISP, an effect that was studied in [16] and tied to the balance between friction and thermal terms in momentum

equation. As for the channel 2 and 3, the increase of the bolometry signal in the simulation is caused by the increased radiance of the plasma due to the injected impurities.

Lack of the effect of B injection on the lower divertor bolometry measurements in the experiments can be attributed to the phenomena not taken into account in the modelling workflow: the most likely candidate for this effect is reduced D and O recycling, which were not modelled here as the wall properties were assumed to be static. In the simulations, B was simply pumped by the wall without affecting the D recycling. A similar discrepancy was found between the T_e measured by the embedded lower divertor Langmuir probes and that estimated from the simulations. In every simulation, B injection resulted in a 2–10 times decrease of the peak T_e^{OSP} , which was not consistent with the experimental results. In the experiment, B powder injection had no effect on T_s , as shown in [6] and in figure 12. Additionally, n_e at the lower divertor increased in the simulations while the experimental measurements slightly decreased [6], further suggesting the reduction

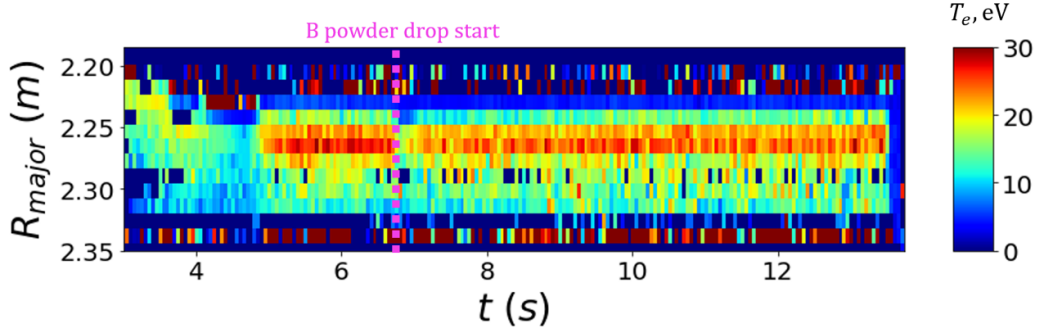


Figure 12. Embedded Langmuir probe measurement of OSP target temperature profile over time.

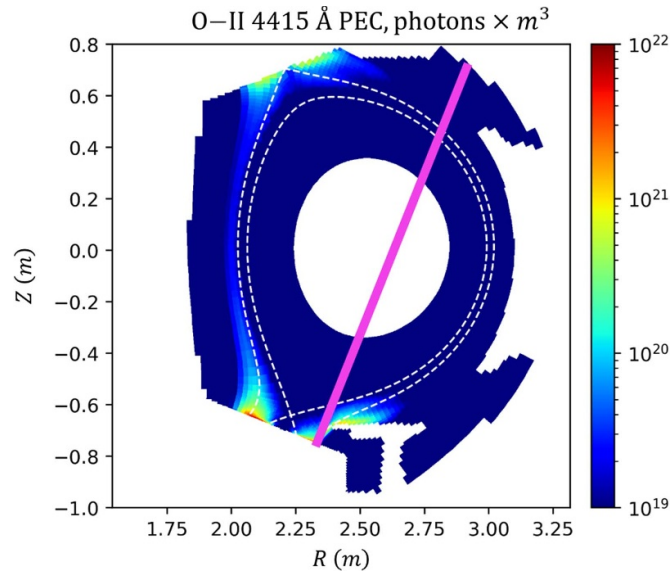


Figure 13. Photon emissivity coefficient for O-II ($\lambda = 4415 \text{ \AA}$) in one of the pre-drop phase simulations (input power $P_{\text{in}} = 2.875 \text{ MW}$, O core concentration $C_{\text{O}}^{\text{core}} = 2.59\%$) and the position of the analysed visible spectroscopy line of sight (width not to scale).

in recycling observed in experiment as a probable cause for the discrepancy.

Another comparison between the B injection effects from the experiment and the SOLEDGE-EIRENE results was made using spectroscopy data for the O-II line brightness at 4415 \AA . As in the case of P_{rad} , an emissivity map for an O ion was calculated based on the parameters of a plasma simulation, and then brightness signals for different lines of sight of a synthetic spectrometer were obtained.

The lower divertor LOS with the brightest O-II signal from shot 56 919 (which happened to be a line near the OSP) was selected for the analysis (figure 13). During shot 56 919, the

injection of B powder resulted in the decrease of the O-II line intensity as was shown in figure 1(d). This was attributed to the reduction of O sputtering due to the B gettering effect [6]. In our modelling, however, the O-II line intensity increases with the addition of a neutral B source (figure 14) despite using the same O source as the core density boundary condition. This result, similar to the bolometry analysis, strengthens the argument that the decrease in O-II line intensity was caused by the O gettering by B and therefore the reduction of O recycling, an effect which could not be modelled in the current workflow, and not by, for example, cooling of the plasma due to the impurity injection. RLP data located upstream from

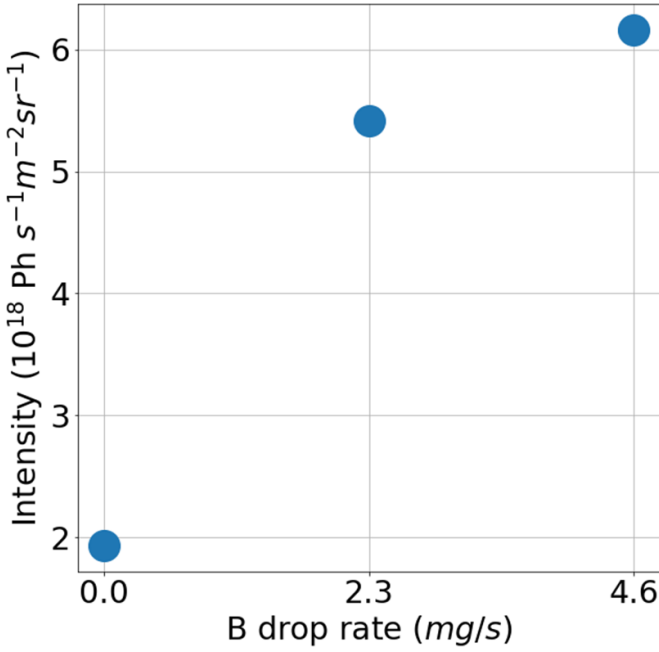


Figure 14. Line intensity for the O-II (441.5 nm) line for simulations with the input power $P_{in} = 2.875$ MW, O core concentration $C_O^{core} = 2.59\%$ and varying B drop rate.

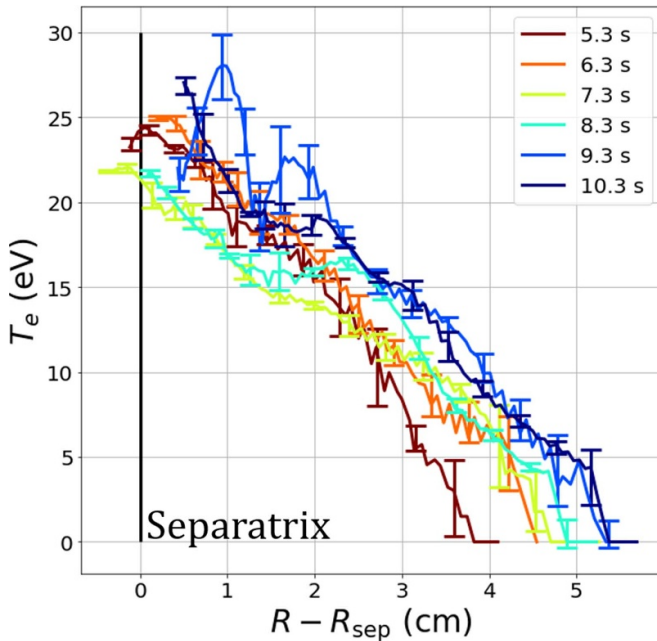


Figure 15. Upstream electron temperature profile from RLP measurements in #56 919 on distance from separatrix. B injection started at $t = 6.7$ s.

the divertor in shot 56 919 demonstrated a decrease in the far SOL T_e while it remained constant near the separatrix (figure 15).

5. Conclusions and future work

A modelling workflow was developed, tested and applied to interpret data from the first IPD experiment on WEST. Pre-drop conditions from experiments were matched qualitatively in D + O SOLEDGE-EIRENE simulations, to which a B source from an evaporated powder particle was then added by modelling with DIS. The impact of a B source on D + O + B simulations was then compared with B injection in the experiment using data obtained from spectroscopy, bolometry and Langmuir probes. The trends in bolometry signal from experiment caused by B injection were matched only at the upper divertor, providing insights into possible physical phenomena that may govern the impact of B powder on plasma parameters. The model suggested a substantial B incident flux to the upper divertor, which could not be compared to experiment due to the lack of visible spectroscopy coverage in that region. The model also suggested the much larger B incident flux to the baffle than to the OSP, which implies that modelling the B recycling and O gettering effects is necessary to improve the interpretive capabilities of this novel workflow. A similar result was obtained in [16] where B was also assumed to not recycle: B deposition distribution peaked at around 15 cm outwards from both strike points. For the OSP in our simulations the wall distance is bigger because baffle overshadows the immediate vicinity of the OSP. B injection in experiment led to the decrease of the O-II line intensity as opposed to simulations O-II line intensity increased. This may be explained by the lack of gettering effect and co-deposition of O in our model. Insensitivity of lower divertor Langmuir probe measurements of n_e , T_e to B injection in experiment and their sensitivity in the numerical models shows that the effect of B powder on D recycling and O gettering effects is a fundamental aspect that has to be included in the future modelling efforts.

The distribution of B particle flux on PFCs in numerical modelling was found to be insensitive to the explored range of input parameters. The addition of B recycling might change this result. Moreover, this property should also be explored in the experiments by, for example, injecting B powder with varying isotope content in different plasma conditions and analysing deposition layers on PFCs through post-mortem analysis, a technique that was used in [28]. If the insensitivity of B incident flux is confirmed, then WEST scenarios that homogenize the B particle flux over the various PFCs should be developed (for example, limiter plasma configuration to redeposit already injected B or to better distribute B during injection).

In order to improve B transport modelling, the workflow can be enhanced by switching to a 3D plasma model to account for non-axisymmetry of the B source and PFCs and/or turbulent transport, as SOLEDGE-EIRENE allows for 3D modelling in a multi-fluid approach [29]. Other potential ways to better match experimental data are to include cross-field drifts or to imitate effects, caused by the changing wall properties, e.g. to reduce D/O recycling in drop phase to match lower divertor temperature and P_{rad} with the experimental values, or












to reduce $C_{\text{O}}^{\text{core}}$ to match decrease of VUV spectroscopy measurements in drop phase in the experiment.

Acknowledgments

This research was supported by the U.S. DOE under Contract No. DE-AC02-09CH11466 with Princeton University.

This work has been carried out within the framework of the EUROfusion Consortium, funded by the European Union via the Euratom Research and Training Programme (Grant Agreement No. 101052200—EUROfusion). Views and opinions expressed are however those of the author(s) only and do not necessarily reflect those of the European Union or the European Commission. Neither the European Union nor the European Commission can be held responsible for them.

ORCID iDs

K. Afonin  <https://orcid.org/0000-0002-5479-2897>
 A. Gallo  <https://orcid.org/0000-0002-7472-7830>
 Y. Marandet  <https://orcid.org/0000-0002-9970-538X>
 G. Bodner  <https://orcid.org/0000-0003-2497-9172>
 P. Devynck  <https://orcid.org/0000-0001-6752-9345>
 A. Diallo  <https://orcid.org/0000-0002-0706-060X>
 J. Gaspar  <https://orcid.org/0000-0003-0104-1616>
 R. Guirlet  <https://orcid.org/0000-0002-5738-5082>
 R. Lunsford  <https://orcid.org/0000-0003-3588-6801>
 F. Nespoli  <https://orcid.org/0000-0001-7644-751X>
 E.A. Unterberg  <https://orcid.org/0000-0003-1353-8865>

References

- [1] Bucalossi J. et al 2014 *Fusion Eng. Des.* **89** 7–8
- [2] Bourdelle C. et al 2015 *Nucl. Fusion* **55** 063017
- [3] Winter J. et al 1989 *J. Nucl. Mater.* **162–164** 713–23
- [4] Toyoda H., Isozumi T., Sugai H. and Okuda T. 1989 *J. Nucl. Mater.* **162–164** 732–6
- [5] Nagy A., Bortolon A., Mauzey D.M., Wolfe E., Gilson E.P., Lunsford R., Maingi R., Mansfield D.K., Nazikian R. and Roquemore A.L. 2018 *Rev. Sci. Instrum.* **89** 10K121
- [6] Bodner G. et al 2022 *Nucl. Fusion* **62** 086020
- [7] Dejarnac R., Sestak D., Gunn J.P., Firdaouss M., Greuner H., Pascal J.-Y., Richou M. and Roche H. 2021 *Fusion Eng. Des.* **163** 112120
- [8] Clairet F., Bottureau C., Chareau J.M. and Sabot R. 2003 *Rev. Sci. Instrum.* **74** 1481–4
- [9] Meyer O. et al 2015 *First EPs Conf. on Plasma Diagnostics (Frascati (Rome), Italy, 14–17 April 2015)* (<https://doi.org/10.22323/1.240.0060>)
- [10] Devynck P., Fedorczak N., Mao R. and Vartanian S. 2021 *J. Phys. Commun.* **5** 095008
- [11] Vallet J.C. et al 1999 Bolometry and radiated power on Tore Supra 26th *EPS Conf. on Plasma Physics (Maastricht, Netherlands, 14–18 June 1999)* (available at: <https://www.osti.gov/etdeweb/biblio/21329019>)
- [12] Shoji M., Kawamura G., Romazanov J., Kirschner A., Eksaeva A., Borodin D., Masuzaki S. and Brezinsek S. 2020 *Nucl. Mater. Energy* **25** 100853
- [13] Feng Y., Sardei F., Grigull P., McCormick K., Kisslinger J., Reiter D. and Igithkanov Y. 2002 *Plasma Phys. Control. Fusion* **44** 611
- [14] Pigarov A.Y. et al 2005 47th Annual Meeting of the Division of Plasma Physics (Denver, USA, 24–28 October 2005) (available at: <https://meetings.aps.org/Meeting/DPP05/Event/36042>)
- [15] Romazanov J. et al 2019 *Nucl. Mater. Energy* **18** 331–8
- [16] Effenberg F. et al 2021 *Nucl. Mater. Energy* **26** 100900
- [17] Bufferand H. et al 2015 *Nucl. Fusion* **55** 053025
- [18] Nespoli F., Kaganovich I.D., Autricque A., Marandet Y. and Tamain P. 2021 *Phys. Plasmas* **28** 073704
- [19] Nespoli F. et al 2023 *Nucl. Fusion* **63** 076001
- [20] Bufferand H. et al 2021 *Nucl. Fusion* **61** 116052
- [21] Faugeras B. 2020 *Fusion Eng. Des.* **160** 112020
- [22] Gallo A. et al 2020 *Nucl. Fusion* **60** 126048
- [23] Di Genova S. et al 2021 *Nucl. Fusion* **61** 106019
- [24] Gallo A. et al 2020 *Phys. Scr.* **2020** 014013
- [25] Afonin K. et al 2022 64th Annual Meeting of the APS Division of Plasma Physics (Spokane, Washington, USA, 17–21 October 2022) (available at: <https://meetings.aps.org/Meeting/DPP22/Session/CP11.57>)
- [26] Devynck P. et al 2021 *Phys. Commun.* **5** 095008
- [27] Mavrin A.A. 2017 *J. Fusion Energy* **36** 161–72
- [28] Krieger K. et al 2023 *Nucl. Mater. Energy* **34** 101374
- [29] Di Genova S. et al 2022 *Nucl. Mater. Energy* **34** 101340